Simultaneous Radio and Physical Mapping for Cellular-Connected UAV by Fusing Radio and Sensing Data

Yuhang Yang*, Xiaoli Xu*, and Yong Zeng*†
*National Mobile Communications Research Laboratory, Southeast University, Nanjing 210096, China
†Purple Mountain Laboratories, Nanjing 211111, China
Email: {yuhang_yang, xiaolixu, yong_zeng}@seu.edu.cn

***Abstract*—Radio map is a promising technology to enable environment-aware wireless communications, which may strengthen the flight safety and enhance communication performance for cellular-connected unmanned aerial vehicles (UAVs). However, conventional interpolation-based radio map construction method relies on the large amount of measurement data and it usually gives poor performance if only limited data along a single UAV flight is available. In this paper, we propose an effective map construction method called *Simultaneous Radio and Physical Mapping (SRaPM)*, which concurrently constructs three closely related radio and physical maps by fusing both radio and sensing data collected by the UAV, namely the link state map (LSM), channel gain map (CGM), and building height map (BHM). Specifically, the received signal strength (RSS) is measured while the UAV receives communication signal from the ground base station (GBS), based on which a hypothesis test problem is solved to determine whether the line of sight (LoS) link is blocked. At the same time, the sensors equipped on the UAV sense the locations of the reflection points, based on which some knowledge about the location and height of the buildings in different directions are deduced. Then, the obtained radio and sensing results are used to update the LSM, CGM and BHM. Numerical results are provided to show the effectiveness of the proposed map construction method as compared with the benchmarking spatial interpolation method.**

I. Introduction

Due to the high mobility, swift deployment and low cost, unmanned aerial vehicles (UAVs) have been widely used in military and civilian fields, such as reconnaissance, transportation, infrastructure inspection, precision agriculture, and disaster relief [1]. To ensure flight safety and support various mission-critical tasks, UAVs are usually equipped with both communication and sensing devices. For instance, a cellular-connected UAV may receive the control information from a remote controller and upload its payload data to the core network via the ubiquitous cellular networks [2]. On the other hand, a multitude of UAV-equipped sensors like camera, radar or lidar, enable the UAV to sense the environment and support various safety functions like collision avoidance.

With the ever-increasing aerial users in future wireless networks, one effective method to strengthen flight safety and enhance the communication performance is via constructing channel knowledge map or radio map [3]–[6]. Most existing radio map construction approaches can be classified into two groups, i.e., *data-driven approach* and *physical map based approach*. With data-driven approach, extensive radio measurements are collected and interpolation-based methods, such as inverse-distance weighted K nearest neighbor (IDW-KNN) [7] and Kriging algorithms [8], are applied to obtain the radio information for locations without measurements. However, such interpolation-based methods ignore the well-established channel models and expert knowledge, and require prohibitive data measurements in complex environments. Therefore, to utilize both measurement data and expert knowledge, some segmented regression approaches of channel models based on Expectation-Maximization (EM) algorithm have been studied for radio map construction [9], [10].

On the other hand, if three dimensional (3D) physical map of the environment is available, the line of sight (LoS)/non-line of sight (NLoS) status along the UAV flying trajectory can be determined, by checking whether there is any building blocking the line segment connecting the ground base station (GBS) and UAV location. Based on such a priori information, statistical channel model can be used to estimate the channel gain [11]. For example, the authors in [4], [12] proposed the concept of virtual segmented obstacle maps for radio map construction. By utilizing the 3D physical obstacle map and applying the segmented regression approaches of channel models based on EM algorithm, the virtual segmented obstacle maps can be obtained. Moreover, with accurate 3D physical map, the boundaries of LoS/NLoS regions can be determined to use the total variation norm minimization (TVNM)-based interpolation, thus speeding up ray-tracing software to construct the accurate radio map [13].

In summary, both data-driven and physical map based approaches for radio map construction have their respective drawbacks. The former incurs significant construction cost for data collection and the spatial interpolation based methods usually neglect the abrupt change of environment, such as building edges. The latter approaches rely on accurate 3D physical map, which may not be always available.

Instead of taking the availability of physical map as granted, the authors in [14] proposed a method to construct the physical map, based on which the radio map is constructed with statistical channel model. To obtain the physical map, extensive radio measurements are required to get the received signal strength (RSS) values and the LoS/NLoS status at different locations within the area. The authors in [11] proposed a probabilistic-

based framework that fuses radio measurement data and Lidar depth measurement data to simultaneously construct physical and radio maps. However, the incorporation of the radio and sensing measurements based on the probabilistic framework incurs large computational complexity, which is difficult to be implemented in real-time.

To overcome the shortcomings of the aforementioned methods, in this paper, we propose a method to construct the radio map and physical map simultaneously, by fusing the real-time radio and sensing measurements data collected by the UAVs in a single flight. The proposed method, termed Simultaneous Radio and Physical Mapping (SRaPM), can be implemented in an online manner, thus is quite appealing for improving the communication performance and strengthening flight safety of aerial users. Specifically, the RSS is measured while the UAV receives information from the GBS, based on which a hypothesis test problem is solved to determine whether the LoS link is blocked. At the same time, the sensors equipped on the UAV estimate the location of the reflection points, based on which some knowledge on the height and location of the buildings in different directions are deduced. Then, the radio and sensing results are used to update the LSM, CGM and BHM by exploiting their inherent relationships. Finally, numerical results are provided to verify the effectiveness of the proposed map construction method as compared with the benchmarking spatial interpolation method.

II. System model

As shown in Fig. 1, we consider a cellular-connected UAV communication system, for which the UAV is equipped with both communication and sensing devices. Radio and physical maps are concurrently constructed based on the measured RSS and sensing results while the UAV flies along a given trajectory to complete certain tasks, e.g., area surveillance.

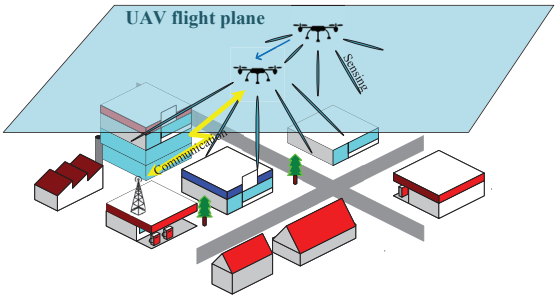

Fig. 1: UAV communication and sensing model.

The region of interest is denoted by a 3D cubic $\mathcal{G} = [0, l_x] \times [0, l_y] \times [0, l_z]$. We assume that the UAV flies in a plane with a constant altitude, denoted by h, which is above the highest building in the area of interest. The trajectory of the UAV projected on the horizontal plane is denoted by $\mathbf{q}(t) = (x(t), y(t)) \in \mathbb{R}^{1\times 2}, 0 \le t \le T$. As the UAV flies, it maintains a communication link with the GBS, located at $\mathbf{q}_B = [x_B, y_B]$ with height h_B, and senses the environment with onboard sensors, e.g., GPS, Radar, Lidar, etc. Based on the radio and sensing measurements, it aims to construct the following closely related radio and physical maps:

- *Link State Map (LSM)*: LSM is represented by the function $\mathcal{L}(x, y)$, which returns the LoS/NLoS status of the communication link between the GBS and the aerial user located at $(x, y, h) \in \mathcal{G}$. Mathematically, we have

$$\mathcal{L}(x,y) = \begin{cases} 1, & \text{if LoS exists at } (x,y,h) \\ 0, & \text{otherwise} \end{cases} \tag{1}$$

- *Channel Gain Map (CGM)*: CGM is represented by the function $\mathcal{G}(x, y)$, which returns the channel gain for the communication link between the GBS and the aerial user located at $(x, y, h) \in \mathcal{G}$.
- *Building Height Map (BHM)*: BHM is represented by the function $\mathcal{H}(x, y)$, which returns the building height at the location (x, y) on the ground.

A. UAV Radio Measurements

For ease of exposition, the mission duration T is discretized into N equally spaced time slot with duration δ_t, i.e., $T = N\delta_t$, such that the change of the communication link between the UAV and the GBS is negligible within each time slot. Thus, the UAV trajectory $\mathbf{q}(t)$ can be approximated by the N-length sequence $\{\mathbf{q}[n], n = 1, ..., N\}$, where $\mathbf{q}[n] = \mathbf{q}(n\delta_t)$. Assume that the GBS has a constant transmitting power. The channel gain measured by the UAV at the nth time slot is determined by the LoS status at the location $\mathbf{q}[n]$ and the distance $d[n]$ between the UAV and GBS, where

$$d[n] = \sqrt{\|\mathbf{q}_n - \mathbf{q}_B\|^2 + (h - h_B)^2}. \tag{2}$$

We adopt the $\alpha\beta$-path loss model, for which the channel gain in dB measured by the UAV in the nth time slot is given by

$$\begin{aligned} g[n] &= f(\alpha_o, \beta_o, \eta_o, \mathbf{q}[n]) \\ &= \beta_o - 10\alpha_o \log_{10}(d[n]) + \eta_o, o \in \{LoS, NLoS\}, \end{aligned} \tag{3}$$

where α_o and β_o represents the path loss exponent and offset, respectively; η_o is a random variable that captures the effect of shadowing, distributed according to $\mathcal{N}(0, \sigma_o^2)$.

Based on the measured channel gain in (3), the UAV may update the CGM value for those locations along its flying trajectory, i.e., $\mathcal{G}(\mathbf{q}[n]) = g_o[n]$. Furthermore, when the channel parameters $\{\alpha_o, \beta_o, \sigma_o^2\}$ for $o \in \{LoS, NLoS\}$ are known, the UAV can determine the link status by solving the following hypothesis test problem

$$\mathbf{P1}: \begin{cases} H_0 : g[n] = f(\alpha_{\text{LoS}}, \beta_{\text{LoS}}, \eta_{\text{LoS}}, d[n]) \\ H_1 : g[n] = f(\alpha_{\text{NLoS}}, \beta_{\text{NLoS}}, \eta_{\text{NLoS}}, d[n]). \end{cases} \tag{4}$$

This is a classical detection problem that can be solved by standard method [15]. Considering that the shadowing is modelled by a zero mean random variable in both LoS and NLoS scenarios, we solve (4) by simply comparing the measured channel gain $g[n]$ with the path loss $\beta_o - 10\alpha_o \log_{10}(d[n])$ where $o \in \{LoS, NLoS\}$. If H_0 is returned by $\mathbf{P1}$, we set $\mathcal{L}(\mathbf{q}[n]) = 1$, and set $\mathcal{L}(\mathbf{q}[n]) = 0$ otherwise. The result of the hypothesis test gives the value $\mathcal{L}(\mathbf{q}[n])$ for the LSM.

Note that since the trajectory of UAV only covers a small portion of the area of interest, the pure channel measurements are typically insufficient to construct high-quality radio maps of

the whole area. Fortunately, by utilizing the spatial geometry semantics and UAV sensing results, the above issues can be addressed, as elaborated in Section III.

B. UAV Sensing Measurements

To sense the environment, the radar sensor equipped on the UAV may transmit beams towards different directions with azimuth angle $\varphi \in (0, 2\pi]$ and zenith angle $\theta \in [0, \theta_{\max}]$. Since the UAV RSS measurement is typically much more frequent than the UAV sensing measurement, we assume that UAV can obtain the environmental sensing measurement once every k time slots, i.e., the sensing results is obtained at the (uk)th time slot, for $u = 1, 2, ..., \lfloor \frac{N}{k} \rfloor$.

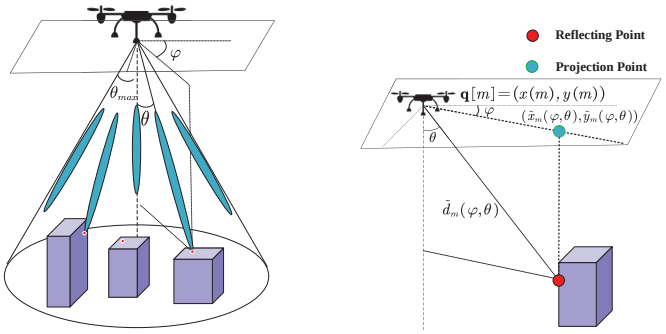

(a) UAV sensing model (b) Reflection point calculation

Fig. 2: An illustration for UAV sensing measurements.

For $m = uk$, the sensing results are obtained with respect to the UAV's current location $\mathbf{q}[m] = (x[m], y[m])$, as shown in Fig. 2. Denote the distance of the reflection point along the direction (φ, θ) by $\tilde{d}_m(\varphi, \theta)$. Then, we can obtain the coordinate of reflection point along the direction (φ, θ) as $(\tilde{x}_m(\varphi, \theta), \tilde{y}_m(\varphi, \theta), \tilde{z}_m(\varphi, \theta))$, where

$$\begin{aligned} \tilde{x}_m(\varphi, \theta) &= x[m] + \tilde{d}_m(\varphi, \theta) \sin(\theta) \cos(\varphi) \\ \tilde{y}_m(\varphi, \theta) &= y[m] + \tilde{d}_m(\varphi, \theta) \sin(\theta) \sin(\varphi) \\ \tilde{z}_m(\varphi, \theta) &= h - \tilde{d}_m(\varphi, \theta) \cos(\theta) \end{aligned} \tag{5}$$

The existence of the reflection point at $(\tilde{x}_m(\varphi, \theta), \tilde{y}_m(\varphi, \theta), \tilde{z}_m(\varphi, \theta))$ implies that the building height at the location $(\tilde{x}_m(\varphi, \theta), \tilde{y}_m(\varphi, \theta))$ should be no smaller than $\tilde{z}_m(\varphi, \theta)$. This provides us the information for updating the BHM, i.e.,

$$\mathcal{H}(\tilde{x}_m(\varphi, \theta), \tilde{y}_m(\varphi, \theta)) \geq \tilde{z}_m(\varphi, \theta). \tag{6}$$

However, limited by the UAV trajectory, (6) can only provide the building height information for a small portion of the area, which is insufficient for the BHM construction. This issue can be addressed by exploiting the spatial geometry semantics and fusing both the radio and sensing data, as elaborated in the following.

III. Simultaneous Radio And Physical Mapping

In this section, we propose a framework for simultaneously constructing the LSM, CGM and BHM by jointly utilizing the UAV radio and sensing measurements data, together with the inherent relationship among these maps, as illustrated in Fig. 3. For instance, if the LoS link is not blocked, it implies that all the buildings along the line segment connecting the GBS and the UAV are of heights lower than the line. This allows us to update the BHM based on LSM. On the other hand, the BHM can be used to improve the accuracy of the hypothesis test in (4) by providing a priori information of the environment, and allow us to infer the link status for those unvisited locations. Furthermore, if the link status of a particular location is determined, we can estimate the channel gain based on (3). This allows us to enhance the CGM based on LSM.

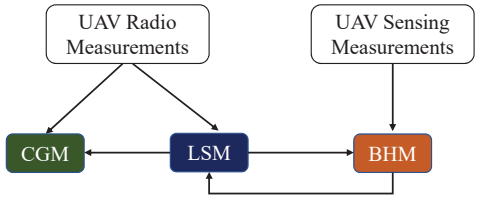

Fig. 3: The proposed framework for simultaneous radio and physical mapping by fusing radio and sensing measurement data.

In the following, we will discuss the inherent relationship among the maps in details and provide a general algorithm for constructing them simultaneously by fusing the UAV radio and sensing data collected as it flies along the trajectory $\{\mathbf{q}[n]\}$.

A. Map Initialization

For convenience, the area of interested is divided into grids with side length δ_d. The link status, channel gain and building height for the points within each small grid are assumed to be the same. Hence, constructing the LSM $\mathcal{L}(x, y)$, CGM $\mathcal{G}(x, y)$, and BHM $\mathcal{H}(x, y)$ is equivalent to determine the value of $\mathcal{L}(x_i, y_j)$, $\mathcal{G}(x_i, y_j)$ and $\mathcal{H}(x_i, y_j)$, with (x_i, y_j) be the center of the (i, j)th grid, for all i, j. Before the UAV is dispatched, it may initialize the maps as

$$\mathcal{L}(x_i, y_j) = 1, \mathcal{G}(x_i, y_j) = 0, \mathcal{H}(x_i, y_j) = 0, \forall i, j. \tag{7}$$

Note that for the LSM, an initial value of 1 means that the UAV-GBS link is dominated by the LoS link in all locations. This is consistent with the initialization of BHM.

B. Map Update Based on Radio Data

As discussed in Section II-A, the UAV can update the CGM and LSM based on the radio measurements $\{g[n], n = 1, ..., N\}$ and the hypothesis test in (4), respectively. Specifically, if $\mathbf{q}[n] \in \left[x_i - \frac{\delta_d}{2}, x_i + \frac{\delta_d}{2}\right) \times \left[y_j - \frac{\delta_d}{2}, y_i + \frac{\delta_d}{2}\right)$, we can set

$$\mathcal{G}(x_i, y_j) = \mathcal{G}(\mathbf{q}[n]) = g[n]. \tag{8}$$

With the value of CGM, the value of LSM $\mathcal{L}(\mathbf{q}[n])$ can be updated by solving the hypothesis testing problem of $\mathbf{P1}$.

Besides, as shown in Fig. 4(a), we denote the location of the GBS antenna as point O and its projection on the UAV flying plane by point A. If the channel between the UAV and GBS is identified to be LoS, the locations on the line connecting $\mathbf{q}[n]$ and point A must also have LoS links, based on the spatial geometry semantics. Similarly, if the channel between the UAV and GBS is identified to be NLoS, then the locations on the line beyond $\mathbf{q}[n]$ must also have NLoS links. However, note

that it requires the assumption that the building has no hollow to ensure the rigorous. This is satisfied in most cases.

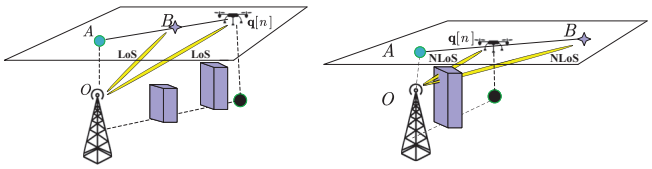

(a) LoS at $\mathbf{q}[n]$ (b) NLoS at $\mathbf{q}[n]$

Fig. 4: An illustration of the LSM and BHM enhancement with radio data.

For any location B on the UAV flight plane, denote by $\Psi(A,B) \subset \{(x_i,y_j), \forall i,j\}$ the set of grids on the line segment connecting point A and B. Further denote by $\bar{\Psi}(A,B,\rightarrow)$ the set of grids along the extension of the line AB towards the direction of B, with line segment AB excluded. Then, the LSM construction method discussed above can be summarized as

$$\mathcal{L}(\Psi(A,\mathbf{q}[n])) = 1, \text{ if } \mathcal{L}(\mathbf{q}[n]) = 1, \tag{9}$$

$$\mathcal{L}(\Psi(A,\mathbf{q}[n],\rightarrow) = 0, \text{ if } \mathcal{L}(\mathbf{q}[n]) = 0. \tag{10}$$

Once the link status of a typical grid is determined, we can estimate the channel gain based on its distance to the GBS, by ignoring the shadowing effect which has zero mean. Mathematically, we have

$$\begin{aligned}&\mathcal{G}(\Psi(A,\mathbf{q}[n])) \\ &= \tilde{f}(\alpha_{\text{LoS}},\beta_{\text{LoS}},\Psi(A,\mathbf{q}[n])), \text{ if } \mathcal{L}(\mathbf{q}[n]) = 1, \end{aligned} \tag{11}$$

$$\begin{aligned}&\mathcal{G}(\Psi(A,\mathbf{q}[n],\rightarrow) \\ &= \tilde{f}(\alpha_{\text{NLoS}},\beta_{\text{NLoS}},\Psi(A,\mathbf{q}[n],\rightarrow), \text{ if } \mathcal{L}(\mathbf{q}[n]) = 0, \end{aligned} \tag{12}$$

where the function $\tilde{f}(\alpha,\beta,\mathbf{q}) = \beta - 10\alpha\log(d(\mathbf{q}_B,\mathbf{q}))$ is the channel gain without shadowing.

Furthermore, if the LoS link between the UAV and GBS exists, as shown in Fig. 4(a), the building heights located in $\Psi(A,\mathbf{q}[n])$ must be lower than the line connecting point O and the UAV at $\mathbf{q}[n]$. Consider $\mathbf{q}' = (x_i', y_j') \in \Psi(A,\mathbf{q}[n])$ as a typical grid that intersect with the line connecting point A and $\mathbf{q}[n]$. The building height at $\mathbf{q}'$ is no greater than

$$\tilde{h}(\mathbf{q}') = \frac{\|\mathbf{q}' - \mathbf{q}_B\|}{\|\mathbf{q}[n] - \mathbf{q}_B\|}(h - h_B) + h_B. \tag{13}$$

This can be used to update the BHM obtained from the UAV sensing results, as

$$\mathcal{H}(\mathbf{q}') = \min\{\mathcal{H}(\mathbf{q}'), \tilde{h}(\mathbf{q}')\}. \tag{14}$$

C. Map Update Based on Sensing Data

As discussed in Section II-B, the sensing results can be used to update the BHM. The sensing results are collected only at the (uk)th time slot, for $u = 1,2,...,\lfloor \frac{N}{k} \rfloor$. For $m = uk$, consider a typical reflection point, denoted by $\mathbf{r}_m = (\tilde{x}_m, \tilde{y}_m, \tilde{z}_m)$. If $\tilde{x}_m \in \left[x_i - \frac{\delta_d}{2}, x_i + \frac{\delta_d}{2}\right)$ and $\tilde{y}_m \in \left[y_j - \frac{\delta_d}{2}, x_j + \frac{\delta_d}{2}\right)$, we can update the BHM as

$$\mathcal{H}(x_i,y_j) = \max\{\mathcal{H}(x_i,y_j), \tilde{z}_m\}. \tag{15}$$

Furthermore, denote the projection of the reflection point on the UAV flying plane by R, i.e., $\mathbf{q}_r = (\tilde{x}_m, \tilde{y}_m, h)$. Then, for the grids along the line segment connecting $\mathbf{q}[m]$ and R, i.e., $\mathbf{q}' \in \Psi(q[m],\mathbf{q}_r)$, the building height is no greater than

$$\tilde{h}_r(\mathbf{q}') = \frac{\|\mathbf{q}' - \mathbf{q}_r\|}{\|\mathbf{q}[m] - \mathbf{q}_r\|}(h_B - \tilde{z}_m) + \tilde{z}_m. \tag{16}$$

The relationship in (16) allows us to update the BHM as

$$\mathcal{H}(\mathbf{q}') = \min\{\mathcal{H}(\mathbf{q}'), \tilde{h}_r(\mathbf{q}')\}. \tag{17}$$

The construction of BHM from the sensing results in (15) can also be used to improve the accuracy of the LSM. As illustrated in Fig. 5, connecting the GBS antenna at point O with the reflection point $\mathbf{r}_m$ gives us a region where the LoS is blocked. Note that it also requires the assumption that the building has no hollow to ensure the rigorous. Denote the intersection of the line with the UAV flying plane by point C. Further consider a point slightly below the reflection point, e.g., $\mathbf{r}_m' = (\tilde{x}_m, \tilde{y}_m, \tilde{z}_m - \varepsilon)$. The intersection of the line connecting O and $\mathbf{r}_m'$ with the UAV flying plane is denoted by point D. Hence, we can conclude that the locations on the line segment CD and the extension towards D must have NLoS link with the GBS. Mathematically, we have

$$\mathcal{L}(\bar{\Psi}(C,D,\rightarrow)) = 0. \tag{18}$$

Note that (18) is not only applicable for determining the link status of those grids that have not been visited, but also help to correct the hypothesis test error for those grids that have been visited by the UAV.

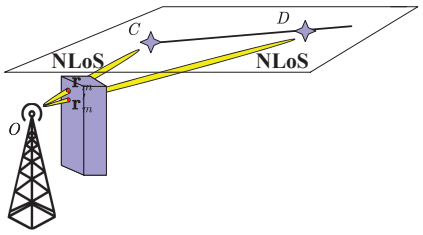

Fig. 5: An illustration of the LSM enhancement with building height information.

D. Proposed SRaPM Construction Algorithm

In Algorithm 1, we summarize the proposed online algorithm for the UAV to simultaneously construct the LSM, CGM and BHM, by fusing the radio and sensing measurements data collected during its flight.

Due to the limitation of the UAV trajectory, updating the LSM, CGM and BHM based on the radio and sensing measurements may not cover the entire area of interest. Denote by Υ_L, Υ_G and Υ_B the set of grids whose link status, channel gain and building height are not updated, respectively. For $\forall(x,y) \in \Upsilon_L$, their initial value will be used, i.e. $\mathcal{L}(x,y) = 1$. Similarly for $\forall(x,y) \in \Upsilon_B$, $\mathcal{H}(x,y) = 0$. Futhermore, for $\forall(x,y) \in \Upsilon_G$, we update the value $\mathcal{G}(x,y)$ according to $\mathcal{L}(x,y)$ and the channel gain model as in (11).

IV. Numerical Results

In this section, numerical results are presented to verify the performance of the proposed algorithm for simultaneous radio and physical map construction. As shown in Fig. 6(a),

Algorithm 1 Simultaneous Radio and Physical Mapping (SRaPM)

Initialize: LSM $\mathcal{L}(x_i, y_j) = 1$, CGM $\mathcal{G}(x_i, y_j) = 0$, BHM $\mathcal{H}(x_i, y_j) = 0, \forall i, j$.
for $n = 1 : N$ **do**
  The UAV collects the radio measurement data $g[n]$ at location $\mathbf{q}[n]$ and determine the link status $\mathcal{L}(\mathbf{q}[n])$ by solving $\mathbf{P1}$.
  if $\mathcal{L}(\mathbf{q}[n]) = 1$ **then**
    Update LSM and CGM according to (9) and (11).
    Update BHM according to (14).
  else
    Update LSM and CGM according to (10) and (12).
  end if
  if $n \mod k = 0$ **then**
    The UAV obtains the sensing measurement data and calculate the reflection points according to (5), at each beam direction.
    for Each determined reflection point **do**
      Update BHM according to (15) and (17).
      Update LSM according to (18).
    end for
  end if
end for
Output: $\mathcal{L}(x_i, y_j)$, $\mathcal{G}(x_i, y_j)$, $\mathcal{H}(x_i, y_j), \forall i, j$

we consider an urban area of size $1\text{km} \times 1\text{km}$ with high-rise buildings, which corresponds to the most challenging environment for coverage-aware UAV navigation, since the LoS/NLoS links and the RSS may alter frequently as the UAV flies. The GBS is located at $\mathbf{q}_B = (500\text{m}, 500\text{m})$ with height 25m and the UAV flight trajectory is a rectangle around the GBS, labeled by the blue line in Fig. 6(a).

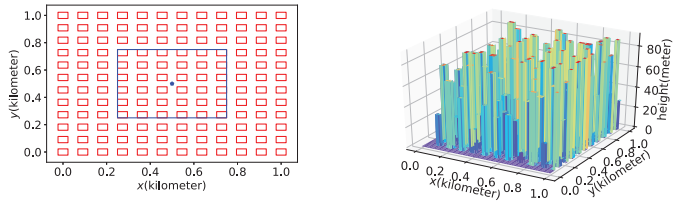

(a) Top view (b) 3D view

Fig. 6: 3D urban environment. The GBS location is labeled as the blue star in the center of the area and the UAV trajectory is labeled as the blue rectangle.

In order to accurately simulate the GBS-UAV channel gain map and 3D building environment map in the given urban environment, we first generate the building locations and heights based on one realization of the statistical model suggested by International Telecommunication Union (ITU) [16], which involves three parameters, namely, a: the ratio of land area covered by buildings to the total land area; b: the mean number of buildings per unit area; and γ: a variable determining the building height distribution, which is modelled as Rayleigh distribution with mean value $\sigma > 0$. We set a maximum value $h_{\max}$ for the height of the building. Fig. 6 shows the 3D and 2D views of the building locations and heights with $a = 0.3, b = 144$ buildings/km^2, and $\gamma = 50$m. For the channel model, we adopt the LoS and NLoS channel parameters as suggested in the 3GPP TR 36.777 urban macrocellular GBS-UAV path loss model [17]. The simulation setup is summarized in Table I.

TABLE I: Main Simulation Parameters

Parameter & notations	Value
The max building height h_{max}	90m
The total distance of the UAV flight trajectory L	2000m
UAV flight height h	100m
The side length of grids δ_d	1m
The path loss exponent α_{LoS} in LoS	2.2
The path loss offset β_{LoS} in LoS	-44.02
The variance of shadowing effects η_{LoS} in LoS	6.25
The path loss exponent α_{NLoS} in NLoS	3.2
The path loss offset β_{NLoS} in NLoS	-30.96
The variance of shadowing effects η_{NLoS} in NLoS	12.25
UAV communication measurement number N	2000
The max UAV sensing elevation angle θ_{max}	90°
The max UAV sensing distance-d_{max}	300m

To evaluate the performance of the proposed map construction algorithm, we consider a benchmark scheme based on the IDW-KNN spatial interpolation. Specifically, for those unvisited grids, their link status are interpolated based on the UAV radio measurements only, with the weights inversely proportional to the distances between the measurement locations and the interpolated grids. After obtaining the complete LSM, the CGM of the unvisited grids can be estimated based on their link status and (11) (12). Fig 7 compares the constructed maps of the proposed method and the benchmark scheme with the ground truth. The proposed SRaPM algorithm is implemented with $k = 5$, i.e., the sensing results are collected every 5 time slots. It is observed that the radio maps constructed with the proposed method match very well with the ground truth. By contrast, the benchmark scheme gives poor performance. This implies that the environment information obtained by UAV sensing is of paramount importance for enhancing radio map quality.

Next, to evaluate the quality of the constructed radio and physical map, we define the root mean square error (RMSE) of the map as the root of the accumulated square error of all the grid values, normalized by the number of grids. For instance, consider typical region divided into $I \times J$ grids. The ground truth CGM is denoted as $\mathcal{G}_{\text{gt}}(x_i, y_j), i = 1, ..., I; j = 1, ..., J$. The RMSE of the constructed map $\mathcal{G}(x_i, y_j)$ is given by

$$\xi_{\mathcal{G}} = \sqrt{\frac{1}{IJ} \sum_{i=1}^{I} \sum_{j=1}^{J} \left(\mathcal{G}_{\text{gt}}(x_i, y_j) - \mathcal{G}(x_i, y_j)\right)^2}. \tag{19}$$

Similarly, we can define the RMSE for the constructed LSM and BHM, denoted as $\xi_{\mathcal{L}}$ and ξ_B, respectively.

Fig. 8 compares the RMSE of the LSM and CGM, constructed based on the proposed SRaPM algorithm and the benchmark scheme. As expected, the proposed algorithm achieves much lower error than the benchmark scheme, thanks to its joint utilization of both radio and sensing data. Furthermore, as k decreases, the quality of the constructed map improves since more environment information is obtained with

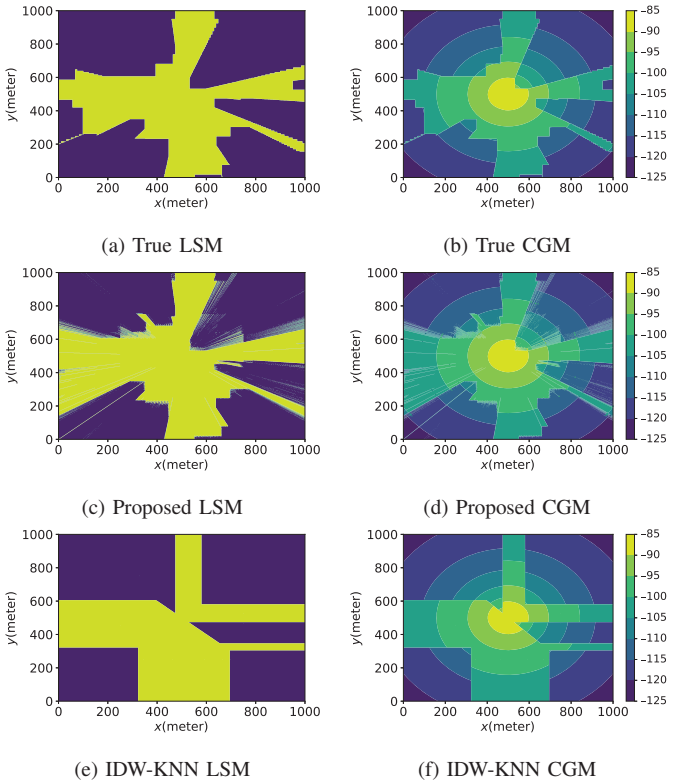

(a) True LSM (b) True CGM

(c) Proposed LSM (d) Proposed CGM

(e) IDW-KNN LSM (f) IDW-KNN CGM

Fig. 7: Comparison of the constructed LSM and CGM with our proposed method and benchmarking spatial interpolation method.

more frequent sensing. Note that the performance of the benchmark scheme does not change with k since it relies on the radio measurements only.

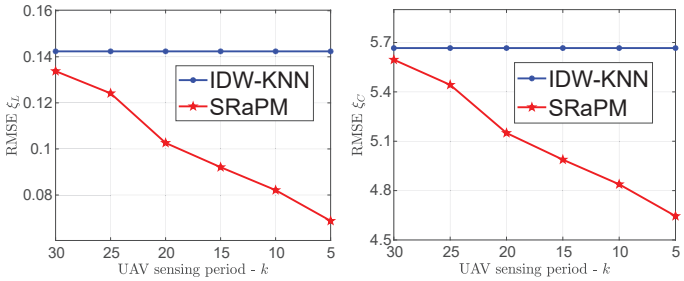

(a) LSM (b) CGM

Fig. 8: Comparison of the RMSE of the constructed maps.

V. Conclusion

In this paper, we proposed an online algorithm for the UAV to simultaneously construct the BHM, LSM and CGM, by fusing the radio and sensing data collected during its flight. Although the visited locations are quite limited along the UAV trajectory, the proposed algorithm is able to construct the map for the whole area by exploiting the inherent relationship between the physical map and the radio map. Furthermore, with the proposed online algorithm, the constructed maps can be enhanced if the additional communication and sensing results are obtained in the new flight. In the future, we will adopt more comprehensive channel models and investigate the 3D radio map construction based on the UAV communication and sensing measurements.

Acknowledgment

This work was supported by the Natural Science Foundation of China under Grant 62071114 and the Natural Science Foundation of Jiangsu Province with grant number BK20200354.

References

[1] H. Shakhatreh, A. H. Sawalmeh, A. Al-Fuqaha, Z. Dou, E. Almaita, I. Khalil, N. S. Othman, A. Khreishah, and M. Guizani, "Unmanned aerial vehicles (UAVs): A survey on civil applications and key research challenges," *IEEE Access*, vol. 7, pp. 48 572–48 634, 2019.

[2] Y. Zeng, Q. Wu, and R. Zhang, "Accessing from the sky: a tutorial on UAV communications for 5G and beyond," *Proceedings of the IEEE*, vol. 107, no. 12, pp. 2327–2375, 2019.

[3] Y. Zeng and X. Xu, "Toward environment-aware 6G communications via channel knowledge map," *IEEE Wireless Commun.*, vol. 28, no. 3, pp. 84–91, Jun. 2021.

[4] J. Chen, O. Esrafilian, D. Gesbert, and U. Mitra, "Efficient algorithms for air-to-ground channel reconstruction in UAV-aided communications," in *2017 IEEE Globecom Workshops (GC Wkshps)*, 2017, pp. 1–6.

[5] Y. Zeng, X. Xu, S. Jin, and R. Zhang, "Simultaneous navigation and radio mapping for cellular-connected UAV with deep reinforcement learning," *IEEE Transactions on Wireless Communications*, vol. 20, no. 7, pp. 4205–4220, 2021.

[6] Y. Huang and Y. Zeng, "Simultaneous environment sensing and channel knowledge mapping for cellular-connected UAV," in *2021 IEEE Globecom Workshops (GC Wkshps)*, 2021, pp. 1–6.

[7] D. Denkovski, V. Atanasovski, L. Gavrilovska, J. Riihijärvi, and P. Mähönen, "Reliability of a radio environment map: Case of spatial interpolation techniques," in *2012 7th international ICST conference on Cognitive Radio Oriented Wireless Networks and Communications (CROWNCOM)*, 2012, pp. 248–253.

[8] E. Dall'Anese, S.-J. Kim, and G. B. Giannakis, "Channel gain map tracking via distributed kriging," *IEEE transactions on vehicular technology*, vol. 60, no. 3, pp. 1205–1211, 2011.

[9] K. Li, P. Li, Y. Zeng, and J. Xu, "Channel knowledge map for environment-aware communications: EM algorithm for map construction," in *2022 IEEE Wireless Communications and Networking Conference (WCNC)*, 2022, pp. 1659–1664.

[10] J. Chen, U. Yatnalli, and D. Gesbert, "Learning radio maps for UAV-aided wireless networks: A segmented regression approach," in *2017 IEEE International Conference on Communications (ICC)*, 2017, pp. 1–6.

[11] O. Esrafilian, R. Gangula, and D. Gesbert, "Map reconstruction in UAV networks via fusion of radio and depth measurements," in *2021 IEEE International Conference on Communications (ICC)*, 2021, pp. 1–6.

[12] B. Zhang and J. Chen, "Constructing radio maps for UAV communications via dynamic resolution virtual obstacle maps," in *2020 IEEE 21st International Workshop on Signal Processing Advances in Wireless Communications (SPAWC)*, 2020, pp. 1–5.

[13] N. Suga, R. Sasaki, M. Osawa, and T. Furukawa, "Ray tracing acceleration using total variation norm minimization for radio map simulation," *IEEE Wireless Communications Letters*, vol. 10, no. 3, pp. 522–526, 2020.

[14] C. Fan, X. Zhong, and J. Wei, "BS-to-ground channel reconstruction with 3D obstacle map based on RSS measurements," *IEEE Access*, vol. 7, pp. 99 633–99 641, 2019.

[15] S. Kay, *Fundamentals of Statistical Signal Processing: Detection Theory*. Prentice-Hall, Upper Saddle River, New Jersey, 1989.

[16] P. Series, "Propagation data and prediction methods required for the design of terrestrial broadband radio access systems operating in a frequency range from 3 to 60 GHz," *Recommendation ITU-R*, pp. 1410–1415, 2013.

[17] G. T. 36.777, "Technical specification group radio access network; study on enhanced LTE support for aerial vehicles," 5G Americas, Tech. Rep., Dec. 2017.